Summary of the 2016/2017 Asian Winter Monsoon

This report summarizes the characteristics of the surface climate and atmospheric/oceanographic considerations related to the Asian winter monsoon for 2016/2017.

Note: The Japanese 55-year Reanalysis (JRA-55; Kobayashi et al. 2015) atmospheric circulation data and COBE-SST (Ishii et al. 2005) sea surface temperature (SST) data were used for this investigation. The outgoing longwave radiation (OLR) data referenced to infer tropical convective activity were originally provided by NOAA. The base period for the normal is 1981 – 2010. The term "anomaly" as used in this report refers to deviation from the normal.

1. Surface climate conditions

Most Asian countries experienced warmer-than-normal conditions throughout boreal winter 2016/2017 (Figure 1.1). Three-month mean temperatures for December 2016 – February 2017 were ranked as very warm across large areas of China, Southeast Asia and western India. Precipitation amounts during the season were above normal in northeastern China, Central Asia, Southeast Asia and Micronesia, and below normal in southwestern China and northern India (Figure 1.2).

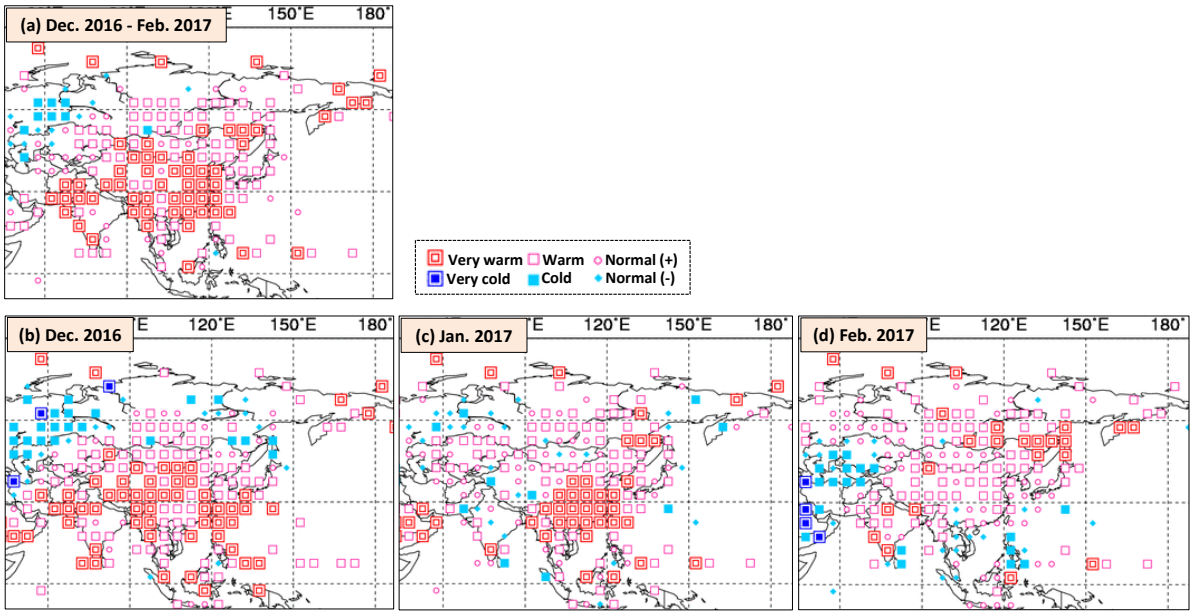

Figure 1.1 (a) Three-month mean temperature anomalies for December 2016 – February 2017, and monthly mean temperature anomalies for (b) December 2016, (c) January 2017 and (d) February 2017

Categories are defined by the three-month/monthly mean temperature anomaly against the normal divided by its standard deviation and averaged in 5° × 5° grid boxes. The thresholds of each category are -1.28, -0.44, 0, +0.44 and +1.28. Standard deviations were calculated from 1981 - 2010 statistics. Areas over land without graphical marks are those where observation data are insufficient or where normal data are unavailable.

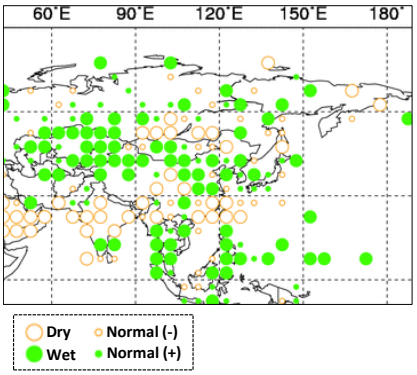

Figure 1.2 Three-month total precipitation ratio for December 2016 – February 2017
Categories are defined by the three-month mean precipitation ratio against the normal and averaged in 5° × 5° grid boxes. The thresholds of each category are 70, 100 and 120%. Areas over land without graphical marks are those where observation data are insufficient or where normal data are unavailable.

Figure 1.3 shows extreme climate events occurring between December 2016 and February 2017. In December, extremely high temperatures were seen in many parts of Mongolia, China, India, Sri Lanka and Pakistan, and extremely high precipitation amounts were observed around the Korean Peninsula. In January, extremely high temperatures were seen over southern China and northern Myanmar, and extremely high precipitation amounts were observed from the southern Indochina Peninsula to northern Sumatra Island. In southern Thailand, more than 90 casualties due to heavy rain were reported in January (European Commission). Precipitation for January at Songkhla in southern Thailand was 682 mm (776% of the 1981 – 2010 normal) according to CLIMAT reports. In February, extremely high temperatures were seen from the southern part of Eastern Siberia to the southeastern part of Central Siberia.

Although most of the season was warmer than normal, cold-air outbreaks were recorded over many parts of East Asia in mid-January and early February (Figure 1.4), bringing heavy snowfall to the Sea of Japan side of western Japan.

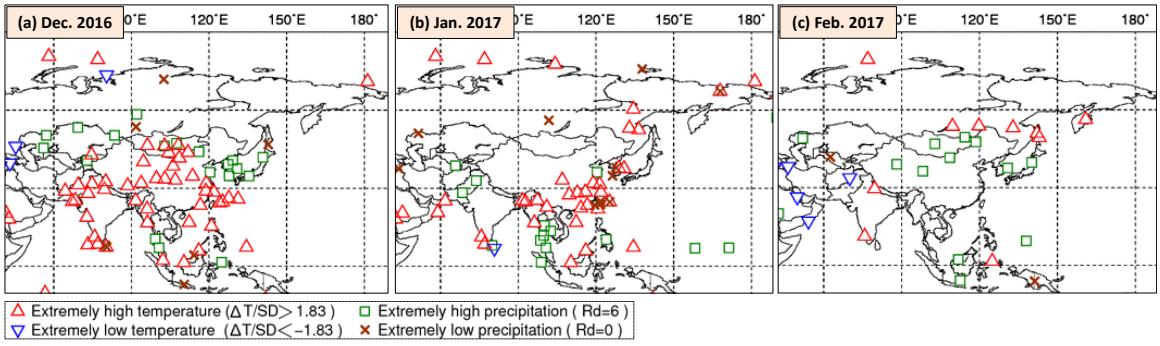

Figure 1.3 Extreme climate events for (a) December 2016, (b) January 2017 and (c) February 2017
Δ T, SD and Rd indicate temperature anomaly, standard deviation and quintile, respectively.

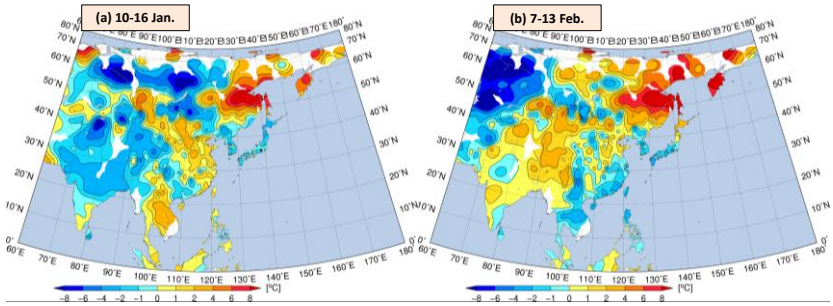

Figure 1.4 Seven-day surface temperature anomalies for (a) 10 – 16 January and (b) 7 – 13 February 2017.
Both are based on SYNOP observation data.

2. Characteristic atmospheric circulation and oceanographic conditions

2.1 Conditions in the tropics

In winter 2016/2017, sea surface temperatures (SSTs) along the equator were above normal in the western Pacific and below normal in the central – eastern Pacific (Figure 2.1). SSTs over the South China Sea to the seas east of the Philippines were higher than normal.

Convective activity inferred from outgoing longwave radiation (OLR) during the season was enhanced in Southeast Asia and suppressed over the Indian Ocean and the equatorial Pacific (Figure 2.2 (a)). In Southeast Asia, where precipitation during this winter was generally categorized as above normal (Figure 1.2), enhanced convection remained throughout the season, especially over the Indochina and Malay peninsulas in December (Figure 2.2 (b)) and January (Figure 2.2 (c)).

In the upper troposphere, clear large-scale divergent anomalies were seen over Southeast Asia in association with enhanced convective activity, and convergent anomalies were observed over the Indian Ocean and the Pacific (Figure 2.3 (a)). In the stream function field (Figure 2.3 (b)), anticyclonic circulation anomalies were centered over southeastern China.

In the lower troposphere, a pair of cyclonic circulation anomalies was observed along the equator over the area from the eastern Indian Ocean to the Maritime Continent (Figure 2.3 (c)). In early January, a cyclonic circulation system with enhanced convection brought heavy rain to southern Thailand (Figure 2.4).

An active convection phase of the Madden-Julian Oscillation (MJO) propagated eastward globally from the latter half of January to February (Figure 2.5 (a)). Southern Oscillation Index values remained near normal during winter.

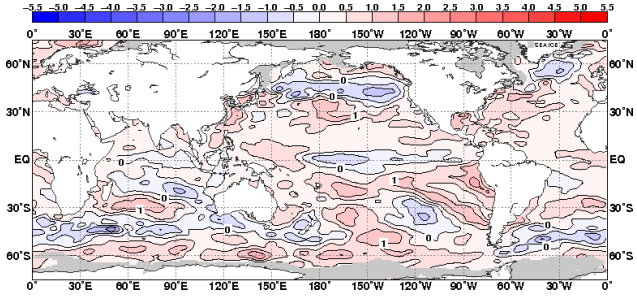

Figure 2.1 Three-month mean sea surface temperature (SST) anomalies for December 2016 to February 2017
The contour interval is 0.5˚C.

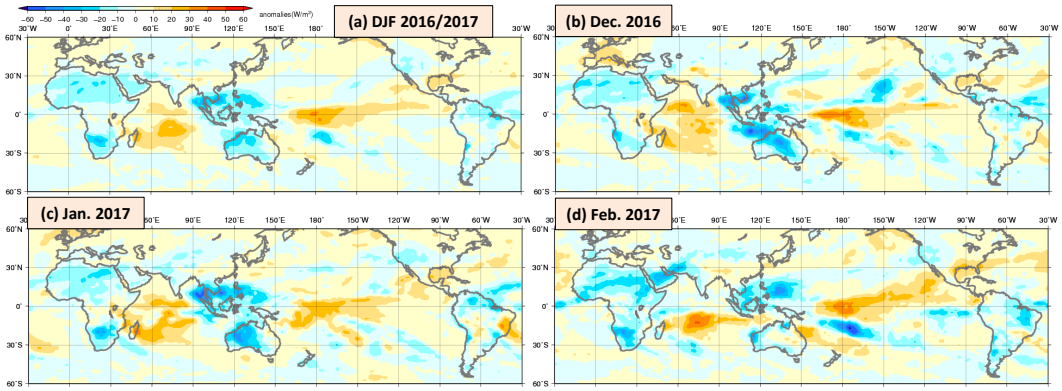

Figure 2.2 Outgoing longwave radiation (OLR) anomalies (a) averaged over the three months from December 2016 to February 2017, and for (b) December 2016, (c) January 2017 and (d) February 2017.
Blue and red shading indicates areas of enhanced and suppressed convective activity, respectively.

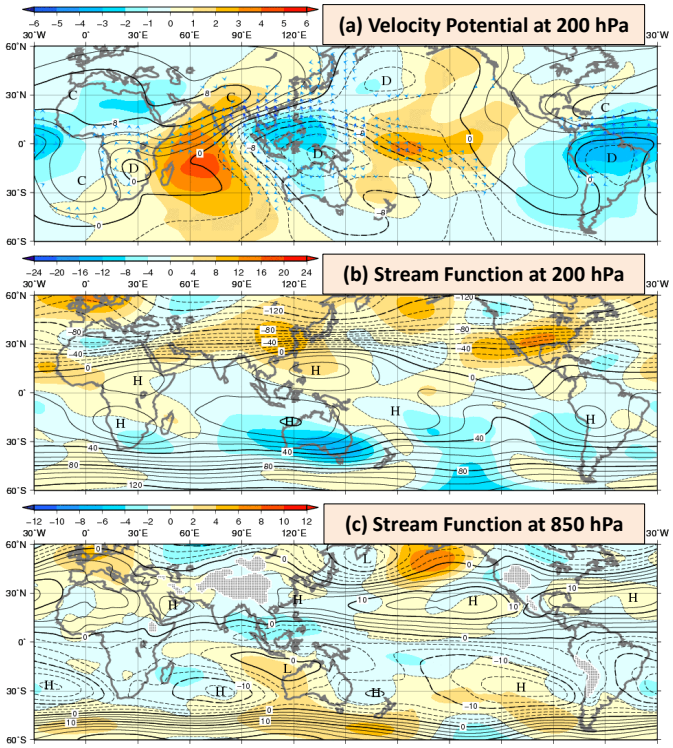

Figure 2.3 Three-month mean (a) 200-hPa velocity potential, (b) 200-hPa stream function, and (c) 850-hPa stream function for December 2016 to February 2017 (unit: 10^6 m^2/s)

(a) The contours indicate velocity potential at intervals of 2 × 10^6 m^2/s, and the shading shows velocity potential anomalies. D and C indicate the bottom and the peak of velocity potential, corresponding to the centers of large-scale divergence and convergence, respectively. (b, c) The contours indicate stream function at intervals of (b) 10 and (c) 2.5 × 10^6 m^2/s, and the shading shows stream function anomalies. H and L denote the centers of anticyclonic and cyclonic circulations, respectively.

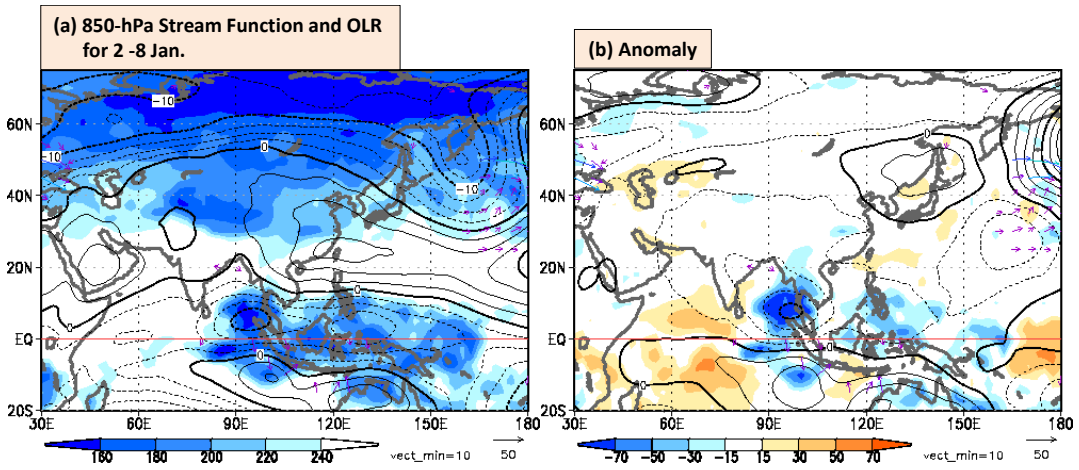

Figure 2.4 (a) Seven-day mean 850-hPa stream function (contours) and outgoing longwave radiation (OLR; shading) for 2 – 8 January 2017, and (b) related anomaly

The thin and thick contour intervals are 2.5 and 10 × 10^6 m^2/s, respectively. Lower OLR values indicate enhanced convective activity except in the mid- and high latitudes. The blue and red shading in (b) indicates areas of enhanced and suppressed convective activity, respectively. Arrows show wave activity fluxes indicating Rossby wave packet propagation.

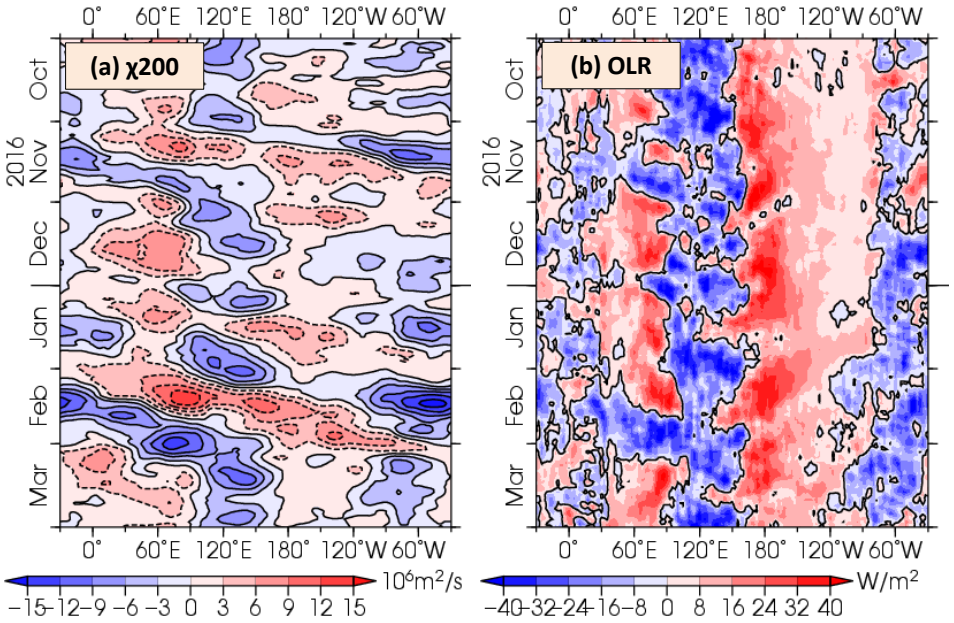

Figure 2.5 Time-longitude cross section of seven-day running mean (a) 200-hPa velocity potential anomalies, and (b) outgoing longwave radiation (OLR) anomalies around the equator (5°S – 5°N) for October 2016 to March 2017
(a) The blue and red shading indicates areas of divergence and convergence anomalies, respectively. (b) The blue and red shading indicates areas of enhanced and suppressed convective activity, respectively.

2.2 Conditions in the extra-tropics and Asian Winter Monsoon

In the 500-hPa height field in winter 2016/2017 (Figure 2.6 (a)), wave trains were seen along the subpolar jet stream over the Eurasian Continent with positive anomalies in northern Europe and northern East Asia, and negative anomalies in Western Siberia and over the seas to the east of Japan. In the sea level pressure field (Figure 2.7 (a)), the Aleutian Low was centered to the west of its normal position. The Siberian High was generally weaker than normal, indicating that the Asian Winter Monsoon was not as active as in normal winters.

Over East Asia, tropospheric temperatures were higher than normal (Figure 2.8) due to the northward meandering of the subpolar jet stream over northern East Asia (Figure 2.6 (a)) and the subtropical jet stream over southern China (Figure 2.3 (b)), causing warmer-than-normal winter conditions (Figure 1).

The subpolar jet stream meandered southward over Western Siberia (Figure 2.6 (a)), where negative sea level pressure anomalies were also centered (Figure 2.7 (a)). This pattern brought southerly warm winds to Siberia and appears to have prohibited Siberian High development.

Figure 2.9 shows that the intraseasonal variability of the Siberian High generally coincides with that of 500-hPa height over Western Siberia. This weaker-than-normal Siberian High was another factor behind the warm conditions seen in East Asia.

In the first half of winter, southerly wind anomalies prevailed over southern China (Figure 2.10), where extreme high temperatures were observed in December and January (Figure 1.3) in association with cyclonic circulation anomalies around Southeast Asia and anticyclonic circulation anomalies to the east of Japan. Northerly cold air flowed into the region less frequently than in normal winters, which contributed to the extreme high temperatures observed over southern China.

As mentioned above, temperatures in mid-January and early February over many parts of

East Asia dropped significantly (Figure 1.4), and heavy snowfall was observed in Japan. During these periods, blocking highs developed around the Bering Sea and migrated westward to Eastern Siberia, and troughs deepened to the south of these highs (Figures 2.11 (a), (d)). In the sea level pressure fields (Figures 2.11 (b), (e)), the Siberian High extended to the eastern coast of the Eurasian Continent and the Aleutian Low also intensified, bringing strong cold-air flow into East Asia (Figures 2.11 (c), (f)).

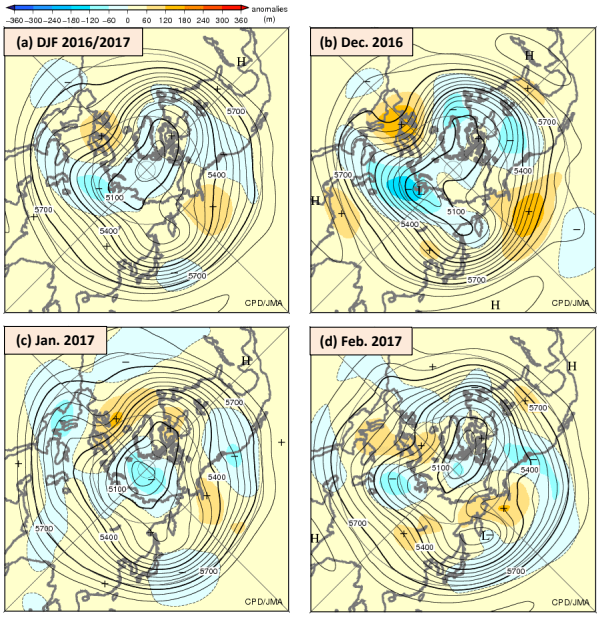

Figure 2.6 500-hPa height (a) averaged over the three months from December 2016 to February 2017, for (b) December 2016, (c) January 2017, and (d) February 2017

The contours indicate 500-hPa height at intervals of 60 m, and the shading denotes anomalies. H and L indicate the peak and bottom of 500-hPa height, respectively, and + (plus) and – (minus) show the peak and bottom of anomalies, respectively.

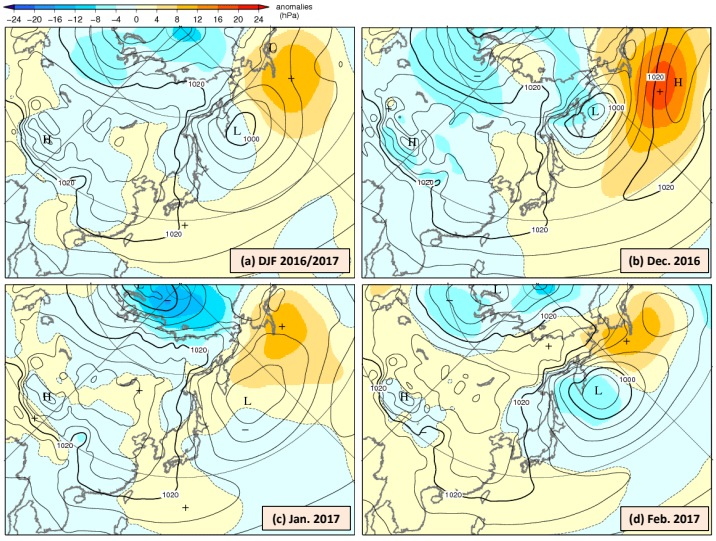

Figure 2.7 Sea level pressure (a) averaged over the three months from December 2016 to February 2017, for (b) December 2016, (c) January 2017 and (d) February 2017

The contours indicate sea level pressure at intervals of 4 hPa, and the shading shows related anomalies. H and L indicate the centers of high and low pressure systems, respectively, and + (plus) and – (minus) show the peak and bottom of sea level pressure anomalies, respectively.

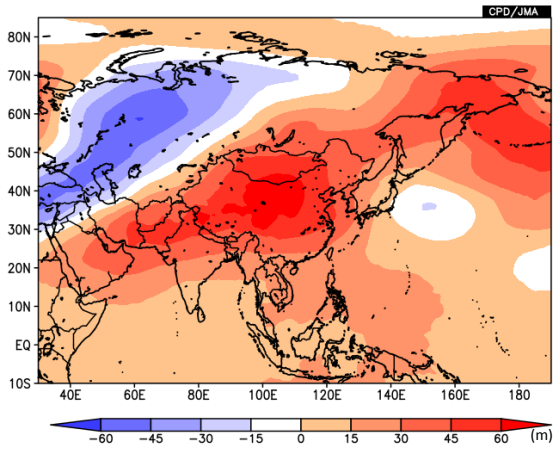

Figure 2.8 Three-month mean anomalies of 300 – 850-hPa height difference for December 2016 to February 2017

Positive values indicate higher-than-normal tropospheric temperatures.

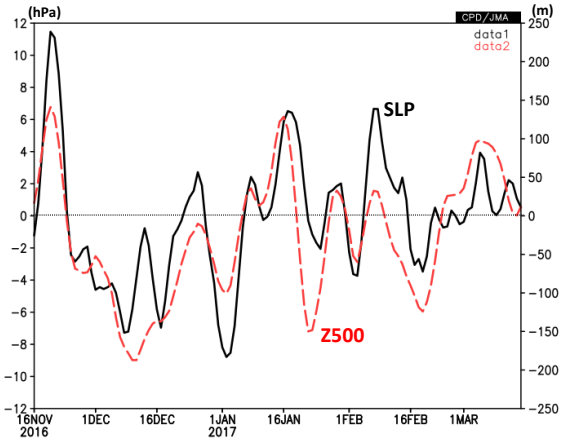

Figure 2.9 Intraseasonal variation of area-averaged sea level pressure anomalies around the center of the Siberian High (40 – 60°N, 80 – 120°E; black; left axis) and 500-hPa height anomalies around Western Siberia (50 – 80°N, 50 – 90°E; red; right axis) from 16 November 2016 to 15 March 2017

Lines indicate five-day running means.

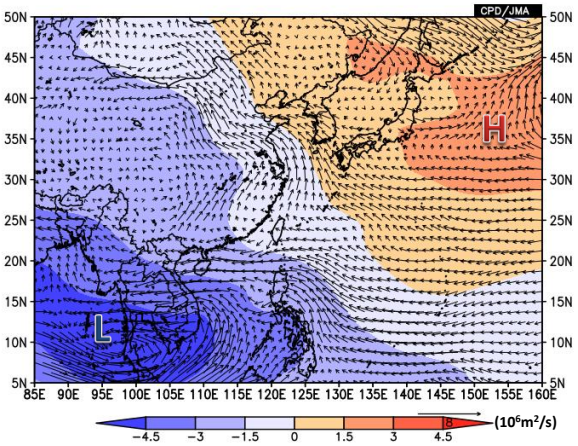

Figure 2.10 850-hPa wind anomalies (arrows) and 850-hPa stream function anomalies (shading) for 1 December 2016 to 10 January 2017

H and L denote the centers of anticyclonic and cyclonic circulation anomalies, respectively.

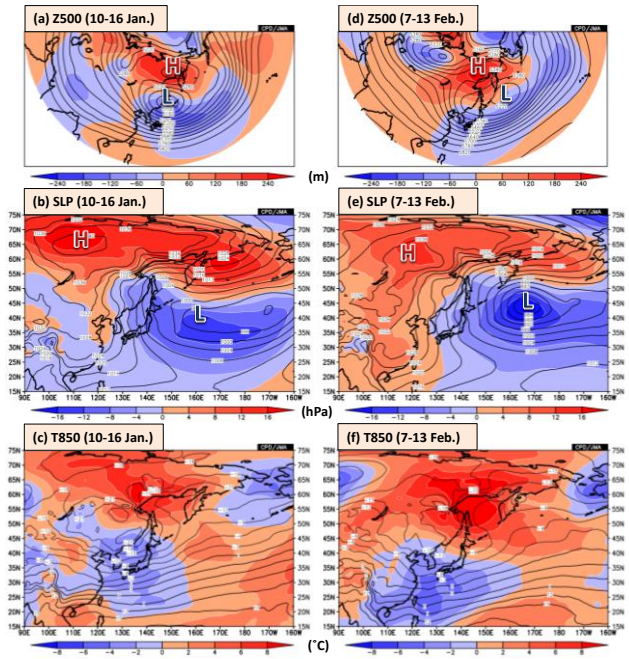

Figure 2.11 ((a), (d)) 500-hPa height, ((b), (e)) sea level pressure and ((c), (f)) 850-hPa temperature for ((a) – (c)) 10 – 16 January and ((d) – (f)) 7 – 13 February 2017

Contours indicate seven-day mean values at intervals of ((a), (d)) 60 m, ((b), (e)) 4 hPa and ((c), (f)) 3°C, and shading denotes related anomalies.

References

Ishii, M., A. Shouji, S. Sugimoto and T. Matsumoto, 2005: Objective Analyses of Sea-Surface Temperature and Marine Meteorological Variables for the 20th Century using ICOADS and the Kobe Collection. Int. *J. Climatol*., **25**, 865-879.

Kobayashi, S., Y. Ota, Y. Harada, A. Ebita, M. Moriya, H. Onoda, K. Onogi, H. Kamahori, C. Kobayashi, H. Endo, K. Miyaoka, and K. Takahashi, 2015: The JRA-55 Reanalysis: General Specifications and Basic Characteristics. *J. Meteorol. Soc. Japan*, **93**, 5 – 48.